Supporting Information

Peters et al. 10.1073/pnas.1306798111

SI Materials and Methods

Active TGF-β Determination and Neutralization. Active TGF-β levels in bronchoalveolar lavage (BAL) fluids from apparently healthy control human subjects and patients with acute respiratory distress syndrome (ARDS) were assessed by a human TGF-β1 ELISA (R&D Systems; DB100B), as per the manufacturer's instructions, or by a dual luciferase reporter bioassay using the firefly luciferase-based TGF-β–responsive $p(CAGA)_{12}$ reporter, and a *Renilla* luciferase standardization reporter (1). TGF-β was neutralized in cell-culture experiments with a pan–TGF-β1, -2, -3-neutralizing antibody (clone 1D11, MAB1835; R&D Systems), as previously described by the authors (2), at a concentration of 10 μg/mL, along with an IgG control antibody also at 10 μg/mL.

Isolated, Ventilated, and Perfused Rabbit Lung. Animal investigations received government approval (Regierungspräsidium Gießen under approval number V54-19c20/15cGI20/10). The isolation and subsequent ventilation and perfusion of rabbit lungs have been described in detail by the authors previously (3). No deviations were made from the described protocol. A standardized procedure was used in all isolated lung studies: lungs were allowed to equilibrate for 30 min, followed by a nebulization step for 10 min to deliver a pretreatment of vehicle, or pharmacological agents. After 20 min, a second nebulization of 10 min delivered TGF-β. After 20 min, a third nebulization of 10 min delivered a 2-mL fluid challenge, which also contained two radioactive tracers, [^{3}H]mannitol (7.2 μCi) and ^{22}NaCl (1.2 μCi), to assess paracellular permeability and $^{22}Na^+$ transit kinetics, respectively. Lung mass and $^{22}Na^+$ were then monitored for 60 min. At the conclusion of the experiment, lungs were lavaged as described previously (4) to assess TGF-β levels and ELF volume. Lung mass was monitored continuously to assess net gain in mass over the experimental time-course, attributable to retention of extravascular lung water. The assessment of $^{22}Na^+$ transit kinetics, resolution of transit kinetics into active and passive components, and calculation of the $K_{f,c}$ have been described by the authors previously (3, 4).

$^{86}Rb^+$ Uptake Studies. Uptake of the K^+ mimic $^{86}Rb^+$ (1 μCi/mL) was used, in combination with the Na^+/K^+-ATPase inhibitor ouabain (1.67 mM) to assess Na^+/K^+-ATPase activity, exactly as described previously (3, 4).

Patch-Clamp of Alveolar Epithelial Cells. To investigate changes in macroscopic current of epithelial cells caused by TGF-β1, the conventional, whole-cell patch-clamp technique on human lung epithelial A549 cells (American Type Culture Collection) and alveolar type II (ATII) cells was performed (4). Stocks of amiloride (Sigma; 10 mM) and benzamil (Sigma; 1 mM) were made in DMSO, whereas TGF-β1 was dissolved in 4 mM HCl to get a 10 μg/mL stock. A549 cells were grown on coverslips for 24–48 h, then on the day of the experiment they were treated for 30 min with vehicle, 1 μM benzamil, 10 ng/mL TGF-β1, or the combination of benzamil and TGF-β1, diluted in the cell medium (DMEM F-12). ATII cells were prepared as described previously (4) and treated similarly. Coverslips were mounted in a flow-through chamber on the stage of an inverted microscope (Axiovert 135; Zeiss) and perfused (2–3 mL/min) with the bath solution containing vehicle, benzamil, or TGF-β1, respectively, by means of a gravity-driven perfusion system. Pipettes pulled from borosilicate glass capillaries (GC 150; Clark Electromedical Instruments) were fire-polished to give a final resistance of 3–5 MΩ. The patch-clamp amplifier was Axopatch 200B (Axon Instruments) and EPC10 (HEKA Elektronik Dr. Schulze). The effective corner frequency of the low-pass filter was 5 kHz. The frequency of digitization was twice that of the filter frequency. The data were stored and analyzed using commercially available software (pCLAMP, Axon Instruments; PatchMaster, HEKA Elektronik Dr. Schulze). Experiments were performed at room temperature. A549 cells were perfused either with: 145 mM NaCl, 2.7 mM KCl, 1.8 mM $CaCl_2$, 2 mM $MgCl_2$, 5.5 mM glucose, 10 mM Hepes, pH 7.4 (bath-1, for experiments with amiloride, SB431542 and PO); or with: 135 mM Na-gluconate, 5 mM KCl, 1 mM $CaCl_2$, 4 mM $MgCl_2$, 10 mM Hepes, 5 mM glucose, 10 mM mannitol, pH 7.4 (bath 2, for experiments with benzamil). Pipettes were back-filled either with: 135 mM potassium methylsulfonic acid, 10 mM KCl, 6 mM NaCl, 1 mM Mg_2ATP, 2 mM Na_2ATP, 5.5 mM glucose, 10 mM Hepes, 1 mM EGTA, pH 7.2 (pipette-1), or 130 mM Na-gluconate, 2 mM Mg_2ATP, 0.647 mM $CaCl_2$, 10 mM Hepes, 1 mM EGTA, 5 mM glucose, pH 7.2 (pipette 2). Whole-cell currents of ATII cells were recorded in essential symmetrical sodium isethionate solutions (bath-3 and pipette-3 solutions). Bath-3 solution contained: 140 mM Na-isethionate, 5 mM K-isethionate, 10 mM Hepes, 1.2 mM $MgSO_4$, 1 mM $CaSO_4$, 5 mM glucose, pH 7.4. Pipette-2 solution contained 140 mM Na-isethionate, 5 mM K-isethionate, 10 mM Hepes, 1.2 mM $MgSO_4$, 1 mM EGTA, 5 mM glucose, pH 7.2. Only those cells containing the granular inclusions typical of type II cell morphology were chosen for the study. Inward and outward currents across the cell membrane were elicited by using a step-pulse protocol from –100 to +60 mV in 10-mV (A549 cells) or 20-mV (ATII cells) increments for a duration of 500 ms or 800 ms (A549 cells) and 100 ms (ATII cells) from a holding potential of –40 mV or 0 mV (A549 cells) or 0 mV (ATII cells). Current–voltage (I–V) relationships were constructed by averaging the current values from 100 to 500 ms or 100–800 ms (A549 cells), and from 20 to 100 ms (ATII cells) from the start of the step pulse and plotted using Origin Software (Microcal Software).

Quantitative Real-Time RT-PCR. Real-time RT-PCR was undertaken exactly as described previously (1) to assess mRNA expression levels in cells and tissue homogenates, using the intron-spanning primers described in Table S1. Expression levels are represented as ΔCt values, using the ubiquitiously expressed, pseudogene-free *hprt* gene as reference.

Immunoblot and Antibodies. The following antibodies were used and were diluted in 5% (wt/vol) nonfat milk powder, unless otherwise indicated: Smad2 (Cell Signaling; 3122; 1:1,000); Smad2/3 (Cell Signaling, 3102; 1:1,000); phospho-Smad2 (Cell Signaling; 3104; 1:1,000); phospholipase D1 [PLD1, Cell Signaling; 3832; 1:1,000 in 1% (wt/vol) BSA in PBS]; phosphatidylinositol-4-phosphate 5-kinase 1α (PIP5K1α; Santa Cruz Biotechnology; 11724; 1:500); NOX4 (NAPDH oxidase 4; a gift from J. Hänze, Philipps University Marburg (5); 1:1,000); FLAG [Sigma, F-3165; 1,000 in 1% (wt/vol) BSA in PBS]; DDDDK-tag [Abcam, ab1257; 1000 in 1% (wt/vol) BSA in PBS]; V5 (Sigma; V-8012; 0.5 μg/mL), rat αENaC (Sigma; E-4652; 1:1,000); Nedd4-2 [Abcam; ab46521 1:2,500 in 5% (wt/vol) BSA in PBST)]; Ubiquitin (Santa Cruz Biotechnology; 8017; 1:5,000); β-Actin (Sigma-Aldrich; A2228, 1:50 000). Protein extracts were boiled, except for the detection of PLD1, where extracts were incubated at 70 °C for 10 min. Pull-down of V5-tagged βENaC for ubiquitination assay: Anti V5 antibody (Sigma-Aldrich;

V8137, 5 μg/800 mg protein). Detection of βENaC with Anti-V5 antibody (Novex by Life Technologies; R96025, 1:2,500 in 5% BSA in PBST).

Site-Directed Mutagenesis. Site-directed mutagenesis was undertaken exactly as described previously (6), using the QuikChange methodology of Stratagene. The primers used are listed in Table S1.

Plasmid Sources and Construction. Plasmids expressing FLAG-tagged mouse α-epithelial sodium channel (αENaC) and γENaC and V5-tagged βENaC were a gift from T. Kleyman, Renal-Electrolyte Division, Department of Medicine, University of Pittsburgh, Pittsburgh (7); wild-type and dominant-negative (K898R) (8) PLD1 were a gift from M. Frohman, Department of Pharmacological Sciences, Stoney Brook University School of Medicine, Stoney Brook, NY; wild-type and dominant-negative (K178A) PIP5K1α were a gift from K. Aoyagi, Department of Life Sciences, Graduate School of Arts and Sciences, University of Tokyo, Tokyo (9). The cloning of the *SCNN1A* (encoding αENaC), *SCNN1B* (encoding βENaC), and *SCNN1G* (encoding γENaC) genes from the human lung has already been reported by the authors (10). These constructs formed the basis of epitope-tagged clones to match the mouse clones described above. The *SCNN1A* and *SCNN1G* genes were amplified from these templates by PCR using the primers listed in Table S1 to generate amplicons that were cloned into the XhoI site of pCMV-Tag4A (Stratagene), generating expression constructs for C-terminal FLAG-tagged αENaC and γENaC, respectively. For βENaC, the XhoI site of pCMV-Tag4 was converted to an AgeI site, followed by a stop codon. The *SCNN1B* open-reading frame was amplified using the primers listed in Table S1 and cloned into the SacII site of pCDNA3.1/V5-His-TOPO (Invitrogen). The βENaC-V5 cassette was excised with NotI and AgeI, and cloned into the modified pCMV-Tag4 to generate an expression construct for a C-terminal V5-tagged βENaC.

Transient Transfection of A549 and Murine Lung Epithelial-12 Cells. All human ENaC constructs were expressed in human A549 cells, whereas mouse ENaC constructs were expressed in mouse lung epithelial (MLE)-12 cells. For transfection, 2.4 μg of DNA was combined with 2.4 μL of Lipofectamine 2000 (Invitrogen) in 2 mL of medium, which was applied to a 70% confluent cell monolayer for 5 h, after which medium was exchanged.

Cell-Surface Biotinylation Studies. Cell-surface biotinylation for ENaC subunits was undertaken essentially as described in ref. 11, using EZ-link Sulfo-NHS-SS-biotin (Pierce) with the following deviations: reactions were quenched with 100 mM glycine in PBS for 30 min (4 °C) before cell lysis, and the biotin pull-down proceeded overnight, not for 2 h. Unless otherwise indicated, both input and biotin pull-down fractions were resolved on the same SDS/PAGE gels, and developed on the same immunoblot, to facilitate comparison of the ENaC subunit bands from the cell-surface fraction with that from the total cellular pool.

PLD Activity Assay. The generation of [^{3}H]phosphatidylbutanol (PBut) and [^{3}H]phosphatidic acid (PA) was assessed exactly as described in ref. 12, after labeling A549 cells with [^{3}H]myristic acid (3 μCi/mL) for 90 min in serum-free DMEM.

RNA Interference Studies. The following siRNA and doses were used in this study (all from Santa Cruz): Smad2 (SC-38374; 50 nM, 24 h) and Smad3 (SC-38376; 50 nM, 24 h), PLD1 (SC-44000; 50 nM, 24 h), PIP5K1α (SC-36232; 150 nM, 24 h), Nedd4-2 (SC-41079; 85 nM, 72 h). Scrambled siRNA was from Ambion (AM4611; 50 nM). For NOX4, the following siRNA were custom synthesized by Biomers.net: 5′-CCU CUU CUU UGU CUU CUAC dTdT-3′ (sense) and 5′-GUA GAC AAA GAA GAGG dTdT-3′ (antisense) (13), and were used at 250 pmol per well of a six-well plate for 72 h.

Assay for H_2O_2 Formation. The generation of reactive oxygen species (ROS) in response to TGF-β stimulation was assessed as a function of H_2O_2 production using a fluorescence-based assay, essentially as described previously (14), with the following deviations: cells were preloaded with 2′,7′-dichlorofluorescein diacetate (H_2DCFH-DA; Molecular Probes) for 30 min at 37 °C in phenol red-free medium. Medium was then replaced with fresh medium containing the relevant pharmacological agent (except for siRNA transfections and EU.K.-134 application, which were performed 24 h before H_2DCFH-DA preloading). After 30-min incubation, medium was replaced with medium containing TGF-β (or vehicle alone) plus the relevant pharmacological agent (or vehicle alone). After 30 min, cells were washed 1× with PBS, before assessment of 2′,7′-dichlorofluorescein (DCF) fluorescence in a microplate spectrofluorimeter at λ_{ex} 485 nm, λ_{ex} 520 nm.

In Vivo Neutralization of TGF-β Signaling. Animal investigations received government approval (Regierungspräsidium Darmstadt under approval number B2/348). The protocol used here is based on that of Zaiman et al. (15) who used an intraperitoneal administration of the SB431542 analog called SD-208 to chronically inhibit TGF-β signaling in the lung in rats. This methodology was very successfully used and demonstrated a role for Tgfbr1/Smad signaling in the pathogenesis of pulmonary arterial hypertension. Our route of administration (oral gavage) and dosing regimen [60 mg/kg, twice daily, in a volume of 100 μL of 1% (wt/vol) methylcellulose dissolved in 0.9% (wt/vol) physiological saline] was identical to that previously established by Zaiman et al. (15). The efficiency of the neutralization of the Tgfbr1/Smad2/3 signaling pathway was demonstrated in the lung parenchyma by assessment of Smad2 phosphorylation. Previously, Zaiman et al. (15) had used an identical Smad2 phosporylation assessment to assess SD-208 efficacy in the pulmonary vasculature. The twice-daily administration fo SD-208 was initiated 24 h after lung injury was induced by bleomycin administration, thus this was a therapeutic regimen. The bleomycin administration to induce lung injury, as a model for ARDS, is a well-established model in our Center, and was used exactly as described previously (16). Similarly, lung wet/dry ratios were calculated exactly as described previously (16).

Use of *nox4*$^{-/-}$ Mice. Animal investigations received government approval (Regierungspräsidium Darmstadt under approval number B2/353). Mice carrying a global deletion of *nox4* have been extensively characterized elsewhere (17). Lung injury was induced in these mice my bleomycin exactly as described previously, and lung fluid balance assessed by wet/dry ration exactly as described above, for the in vivo neutralization of TGF-β signaling.

Flow Cytometry. Flow cytometry was undertaken as described previously by our group (18, 19). Human or mouse ATII cells were cultured for 3 d and treated with brefeldin A and TGF-β as described for A459 cells and ATII cells in the *Cell-Surface Biotinylation* and electrophysiology sections. Departures from our published protocols were restricted to the specific antibodies used: anti-αENaC [Sigma HPA012743 (0.2 mg/mL) subsequently diluted 1:50 in FACS buffer] or a nonimmune isotype-matched antibody (Sigman I-5006; 0.2 mg/mL; subsequently diluted 1:50 in FACS buffer). The secondary antibody was A-21245 [Alexa Fluor 647 Goat Anti-Rabbit IgG (H+L), highly cross-adsorbed] diluted 1:350 in FACS buffer for both nonimmune- and anti-αENaC–treated cells.

Detection of Cysteine Oxidation in βENaC. The A549 cells were seeded in 60-mm cell-cuture dishes and used for the study at 70% confluence. Cells were transfected with for 5 h with 2.4 μg of V5-tagged βENaC- or V5-tagged C43S βENaC-expressing constructs using 6 μL Lipofectamine 2000 transfection reagent (Invitrogen). On the following day, 5 mM 4-(3-azidopropyl)cyclohexane-1,3-dione (DAz-2; Cayman Chemical) was added to the medium, and 15 min later cells were stimulated with 10 ng/mL TGF-β for 30 min. Cells were then washed 3× with PBS and lysed in 100 μL lysis buffer [20 mM Tris·Cl pH 7.5; 150 mM NaCl; 1 mM EDTA; 1 mM EGTA; 0.5% Igepal CA-630 (Nonidet P-40); 1 mM Na_3VO_4 and Complete Protease inhibitor]. After centrifugation at 3,000 × *g* for 20 min at 4 °C, the supernatant was collected and 250 μL of protein was incubated with 200 μM methyl 2-(diphenylphosphino)-4-(15-oxo-19-(2-oxohexahydro-1H-thieno[3,4-d]imidazol-4-yl)-4,7,10-trioxa-14-azanonadecylcarbamoyl)benzoate (Phosphine-biotin; Cayman Chemical) for 1 h at 37 °C with gentle agitation. To pull down proteins containing oxidized cysteine residues, 60 μL of streptavidin beads were added to the reaction and the tubes were rotated overnight at 4 °C. Then, the beads were washed once with 150 mM NaCl; 50 mM Tris pH 7.4; 5 mM EDTA, twice with 500 mM NaCl; 50 mM Tris pH 7.4; 5 mM EDTA and three times with 500 mM NaCl; 20 mM Tris pH 7.4; 0.2% (wt/vol) BSA. After the final wash with 10 mM Tris pH 7.4, 20 μL protein loading buffer was added to the reaction and the supernatant containing purified proteins was subjected to the SDS/PAGE and Western blot along with 5 μg of the input. The V5-tagged βENaC or V5-tagged C43S βENaC were visualized using monoclonal anti V5-tag antibody (Sigma-Aldrich), as described for the regular biotinylations studies described above.

Half-Life Determinations. The surface half-lives of wild-type and C43S βENaC were assessed by pulse-chase methodology exactly as described previously (20), as modified in (21), with cell-surface biotinylation.

1. Alejandre-Alcázar MA, et al. (2007) Hyperoxia modulates TGF-β/BMP signaling in a mouse model of bronchopulmonary dysplasia. *Am J Physiol Lung Cell Mol Physiol* 292(2):L537–L549.
2. Kumarasamy A, et al. (2009) Lysyl oxidase activity is dysregulated during impaired alveolarization of mouse and human lungs. *Am J Respir Crit Care Med* 180(12): 1239–1252.
3. Vadász I, et al. (2005) Thrombin impairs alveolar fluid clearance by promoting endocytosis of Na^+,K^+-ATPase. *Am J Respir Cell Mol Biol* 33(4):343–354.
4. Vadász I, et al. (2005) Oleic acid inhibits alveolar fluid reabsorption: A role in acute respiratory distress syndrome? *Am J Respir Crit Care Med* 171(5):469–479.
5. Goyal P, et al. (2005) Identification of novel Nox4 splice variants with impact on ROS levels in A549 cells. *Biochem Biophys Res Commun* 329(1):32–39.
6. Morty RE, Shih AY, Fülöp V, Andrews NW (2005) Identification of the reactive cysteine residues in oligopeptidase B from *Trypanosoma brucei*. *FEBS Lett* 579(10):2191–2196.
7. Bruns JB, et al. (2003) Multiple epithelial Na^+ channel domains participate in subunit assembly. *Am J Physiol Renal Physiol* 285(4):F600–F609.
8. Hammond SM, et al. (1997) Characterization of two alternately spliced forms of phospholipase D1. Activation of the purified enzymes by phosphatidylinositol 4,5-bisphosphate, ADP-ribosylation factor, and Rho family monomeric GTP-binding proteins and protein kinase C-α. *J Biol Chem* 272(6):3860–3868.
9. Aoyagi K, et al. (2005) The activation of exocytotic sites by the formation of phosphatidylinositol 4,5-bisphosphate microdomains at syntaxin clusters. *J Biol Chem* 280(17):17346–17352.
10. Fronius M, Bogdan R, Althaus M, Morty RE, Clauss WG (2010) Epithelial Na+ channels derived from human lung are activated by shear force. *Respir Physiol Neurobiol* 170(1):113–119.
11. Hanwell D, Ishikawa T, Saleki R, Rotin D (2002) Trafficking and cell surface stability of the epithelial Na^+ channel expressed in epithelial Madin-Darby canine kidney cells. *J Biol Chem* 277(12):9772–9779.
12. O'Luanaigh N, et al. (2002) Continual production of phosphatidic acid by phospholipase D is essential for antigen-stimulated membrane ruffling in cultured mast cells. *Mol Biol Cell* 13(10):3730–3746.
13. Li S, et al. (2008) NOX4 regulates ROS levels under normoxic and hypoxic conditions, triggers proliferation, and inhibits apoptosis in pulmonary artery adventitial fibroblasts. *Antioxid Redox Signal* 10(10):1687–1698.
14. Dada LA, et al. (2003) Hypoxia-induced endocytosis of Na,K-ATPase in alveolar epithelial cells is mediated by mitochondrial reactive oxygen species and PKC-ζ. *J Clin Invest* 111(7):1057–1064.
15. Zaiman AL, et al. (2008) Role of the TGF-beta/Alk5 signaling pathway in monocrotaline-induced pulmonary hypertension. *Am J Respir Crit Care Med* 177(8):896–905.
16. Wygrecka M, et al. (2007) Cellular origin of pro-coagulant and (anti)-fibrinolytic factors in bleomycin-injured lungs. *Eur Respir J* 29(6):1105–1114.
17. Zhang M, et al. (2010) NADPH oxidase-4 mediates protection against chronic load-induced stress in mouse hearts by enhancing angiogenesis. *Proc Natl Acad Sci USA* 107(42):18121–18126.
18. Herold S, et al. (2008) Lung epithelial apoptosis in influenza virus pneumonia: The role of macrophage-expressed TNF-related apoptosis-inducing ligand. *J Exp Med* 205(13):3065–3077.
19. Unkel B, et al. (2012) Alveolar epithelial cells orchestrate DC function in murine viral pneumonia. *J Clin Invest* 122(10):3652–3664.
20. Comellas AP, et al. (2006) Hypoxia-mediated degradation of Na,K-ATPase via mitochondrial reactive oxygen species and the ubiquitin-conjugating system. *Circ Res* 98(10):1314–1322.
21. Lecuona E, Sun H, Vohwinkel C, Ciechanover A, Sznajder JI (2009) Ubiquitination participates in the lysosomal degradation of Na,K-ATPase in steady-state conditions. *Am J Respir Cell Mol Biol* 41(6):671–679.

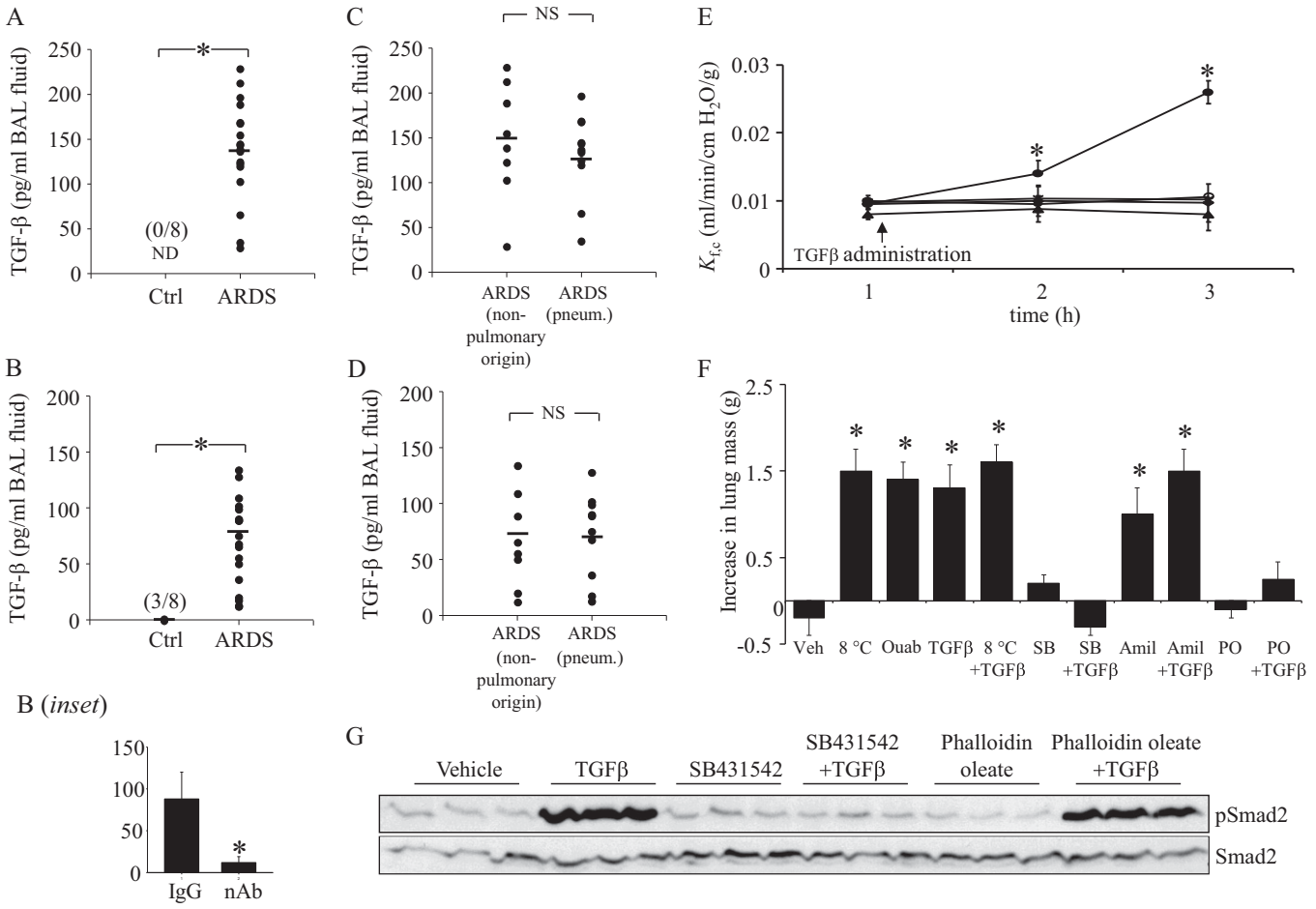

Fig. S1. Active TGF-β is present in the lungs of patients with ARDS, and exogenous TGF-β applied to the alveolar airspaces influences lung fluid retention after fluid challenge, but not endothelial permeability. Active TGF-β levels were assessed by ELISA (*A*) or bioassay (*B*) in BAL fluids from mechanically ventilated patients with ARDS (n = 17) and healthy volunteers (n = 8). The bioassay was performed on ARDS patient samples in the presence of a TGF-β1, -2, -3 neutralizing IgG (nAb) or nonspecific IgG control (IgG) antibody (*Inset*). (*C* and *D*) TGF-β levels in patients with ARDS do not differ between patients groups with pulmonary vs. nonpulmonary origins of lung injury. Active TGF-β levels were assessed by ELISA (*A*) or bioassay (*B*) in BAL fluids from 17 mechanically ventilated patients with ARDS: (*i*) eight patients with ARDS with nonpulmonary origins (sepsis, n = 5; pancreatitis, n = 1; other, n = 2; 53.7 ± 7.7 y; five male/three female; PaO_2/FiO_2, 157.7 ± 21.9); and (*ii*) nine patients with ARDS resulting from pneumonia (47.8 ± 5.0 y; five male/four female; PaO_2/FiO_2, 159.2 ± 20.1). (*E*) The effects of vehicle (open circle), low temperature (8 °C; diamond), TGF-β (10 ng/mL, in the ELF; diamond), amiloride (10 μM, in the ELF; cross), or oleic acid (25 μM in perfusate; closed circle; as positive control) on lung capillary permeability were assessed by capillary filtration coefficient ($K_{f,c}$) (n = 3, per group; * indicates vs. vehicle). Data represent mean ± SD, *$P < 0.05$. The steady-state lung mass (*F*) was assessed in isolated, ventilated, and perfused rabbit lungs pretreated with vehicle (Veh), low temperature (8 °C), ouabain (10 μM), TGF-β, SB431542 (SB), amiloride (Amil), phalloidin oleate (PO), or combinations thereof, 60 min after application of a 2-mL fluid challenge (n = 8, per group; * indicates versus vehicle). (*G*) TGF-β pathway activation assessed by Smad2 phosphorylation (pSmad2) in three representative lungs from *F*.

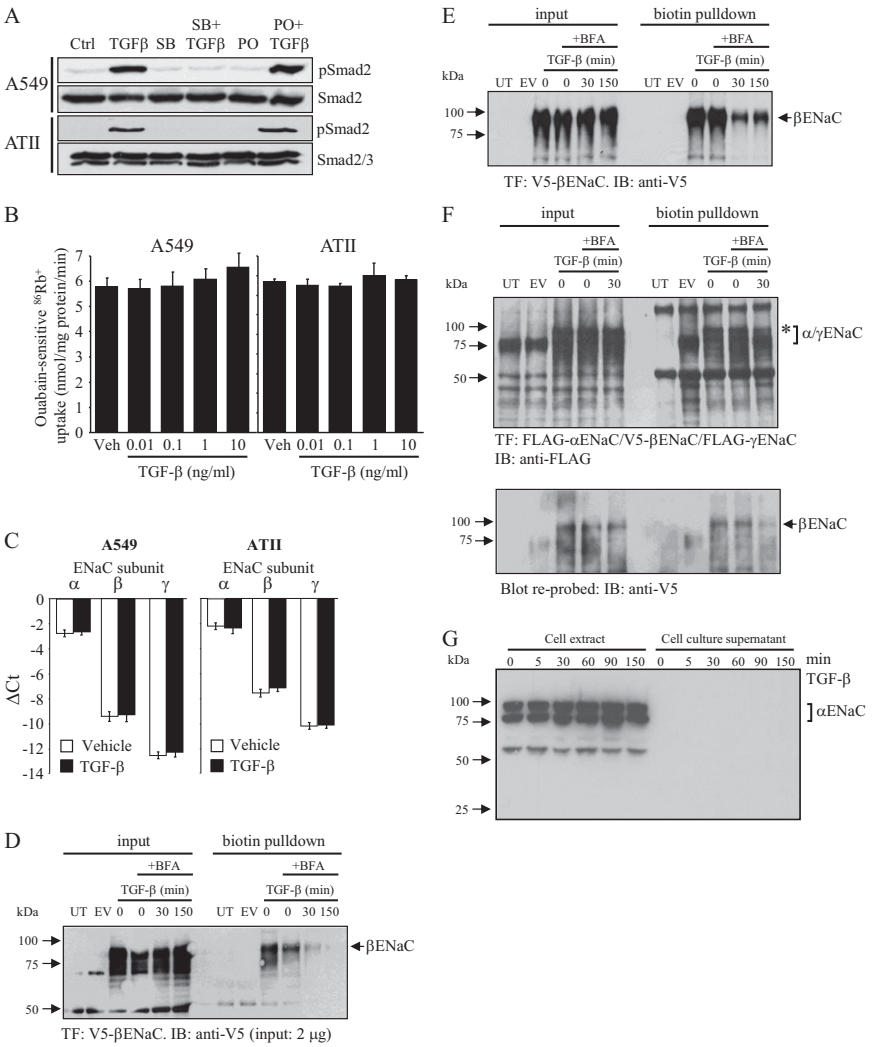

Fig. S2. TGF-β does not impact Na/K-ATPase activity or ENaC subunit expression levels, but does drive endocytosis without plasma membrane shedding of ENaC subunits. (*A*) TGF-β drives Smad2 phosphorylation (pSmad2) in A549 and primary ATII cells. (*B*) TGF-β does not impact ouabain-sensitive $^{86}Rb^{+}$ uptake after 150-min exposure to TGF-β. Effects of TGF-β application (10 ng/mL; 30 min) on ouabain-sensitive $^{86}Rb^{+}$ uptake by A549 and primary mouse ATII cells ($n = 6$, per group) are illustrated. Data represent mean ± SD. (*C*) Levels of mRNA transcripts encoding αENaC (*SCNN1A*), βENaC (*SCNN1B*), and γENaC (*SCNN1G*) assessed by real-time RT-PCR in A549 cells and primary mouse ATII cells with or without TGF-β stimulation. Data represent mean ± SD ($n = 3$, per group). (*D*) Assessment of the impact of TGF-β on cell-surface expression of V5-tagged βENaC in A549 cells. Total levels are evident in input lanes, and cell-surface abundance was assessed by biotinylation, pull-down, and immunoblot (IB) on the same membrane. Cells were pretreated with brefeldin A (BFA; 10 μg/mL), and were untransfected (UT), transfected with empty vector (EV), or transfected (TF) with constructs expressing the epitope-tagged ENaC subunits. This blot is a repeat blot of that presented in Fig. 3*C*, using a 2-μg input in place of 10 μg. (*E*) Mouse lung epithelial MLE-12 cells were transfected with V5-tagged mouse βENaC, and the effect of TGF-β on cell-surface abundance of V5-tagged βENaC assessed. (*F*) A549 cells were transfected with all three tagged ENaC subunits simultaneously, and the effects of TGF-β on surface abundance of FLAG-tagged αENaC and γENaC assessed. Given similar molecular masses, it was not possible to differentiate between αENaC and γENaC; however, a clear reduction in the intensity of the band marked by an asterisk (*) is evident. The same immunoblot was reprobed with an anti-V5 antibody to reveal surface abundance of the βENaC. Data are quantified in Fig. 3*D*. (*G*) Assessment of ENaC shedding into cell-culture supernatants after TGF-β stimulation. A549 cells were treated with TGF-β (10 ng/mL) for the indicated time-point, after which cells and cell-culture supernatants were harvested. Whole-cell homogenates were prepared from cell monolayers, and proteins in cell-culture supernatants were precipitated with trichloroacetic acid, and the pellet washed (3 × 10 min) with cold acetone (4 °C) and air-dried. Protein samples (25 μg) were resolved by SDS/PAGE and blotted to nitrocellulose, after which blots were probed for endogenous αENaC (rabbit anti-rat αENaC; E-4652; Sigma; 1:1,000).

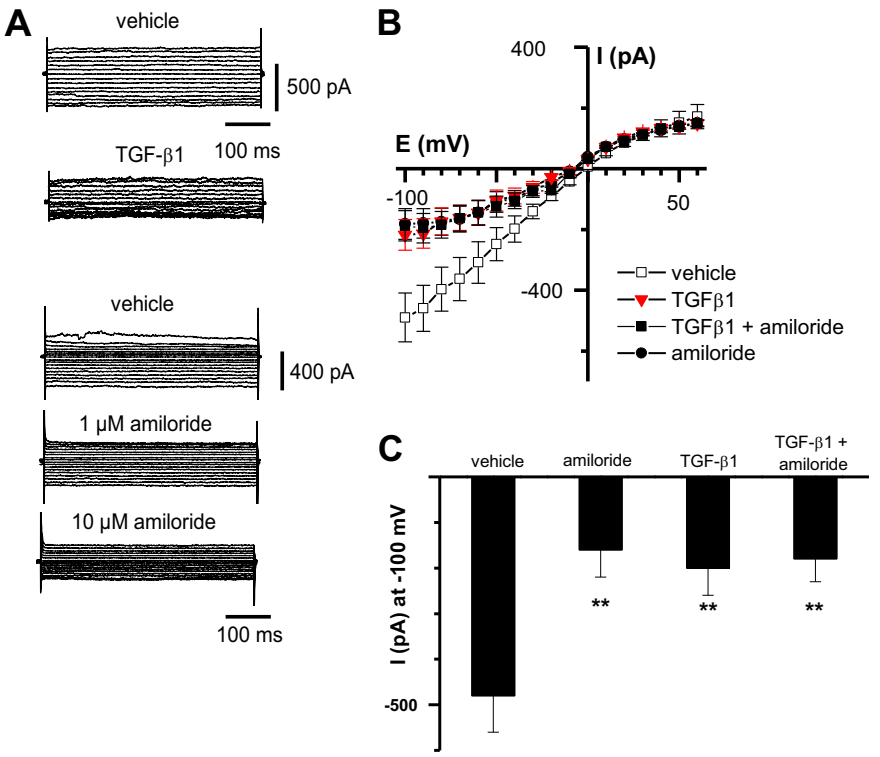

Fig. S3. TGF-β reduced whole-cell sodium currents in A549 cells. (*A*) Representative 500-ms traces demonstrate whole-cell currents in control and after 30-min exposure to TGF-β1 (10 ng/mL). Currents were evoked by applying incremental depolarizing 10-mV voltage steps between −100 and +60 mV from a holding potential of −40 mV. (*B*) Averaged whole-cell I–V plots of total current (open square, vehicle), after TGF-β1 treatment (red triangle), amiloride-treatment (filled circle), and TGF-β plus amiloride-treatment (filled square) ($n = 6$) per group. (*C*) Summarized data of whole-cell current elicited by a test potential at −100 mV in control (vehicle) and after preincubation with amiloride (10 μM), TGF-β1 (10 ng/mL), TGF-β + amiloride ($n = 6$, per group). $^{**}P < 0.01$ in comparison with control.

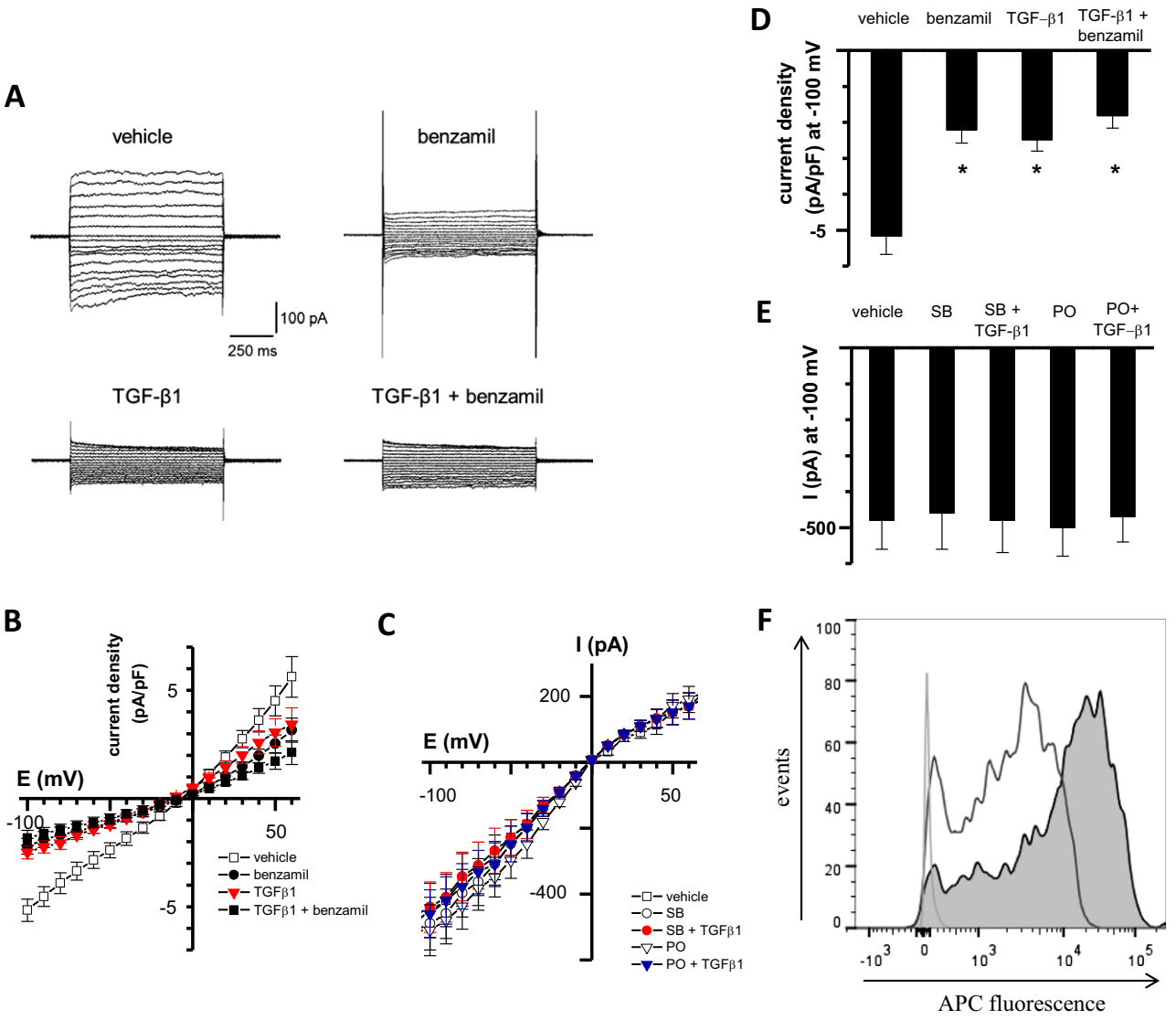

Fig. S4. TGF-β suppresses whole-cell sodium currents in A549 cells. (*A*) Typical whole-cell currents recorded in the absence (vehicle) or after treatment with 10 ng/mL TGF-β, 1 μM benzamil, or the combination of the two. (*B*) Mean current density vs. voltage relationship for cells treated with vehicle (control, $n = 15$), benzamil (1 μM, $n = 9$), and TGF-β (10 ng/mL), in the absence ($n = 10$) and presence of benzamil ($n = 5$). (*C*) Pretreatment with the TGF-β kinase inhibitor SB431542 (SB) or the inhibitor of actin mobility, PO, completely abolished the effect of TGF-β on whole-cell sodium currents in A549 cells. Averaged whole-cell I–V plots of whole-cell current in vehicle (control; open square) -treated cells, or after preincubation with SB431542 (open circle), PO (open triangle), SB431542+ TGF-β (red circle), or PO+TGF-β (blue triangle) ($n = 6$, per group). (*D*) Whole-cell current density at −100 mV in vehicle ($n = 15$) -treated cells, or after treatment with benzamil ($n = 9$), TGF-β ($n = 10$) or TGF-β + benzamil ($n = 5$). *$P < 0.05$ for comparison with control. (*E*) Summarized data of whole-cell currents elicited by a test potential at −100 mV in vehicle treated cells, or after preincubation with SB431542 (10 μM, SB), SB431542+TGF-β, PO (1 μM), or PO+TGF-β ($n = 6$, per group). (*F*) Demonstration of the ability of the αENaC antibody to detect αENaC on the surface of nonpermeabilized mouse ATII cells. The light gray trace represents unstained cells, and the dark gray trace (unshaded plot) represents ATII cells treated with a nonimmune control antibody, and the black trace (shaded plot) represents ATII cells treated with an isotype-matched antibody directed against αENaC.

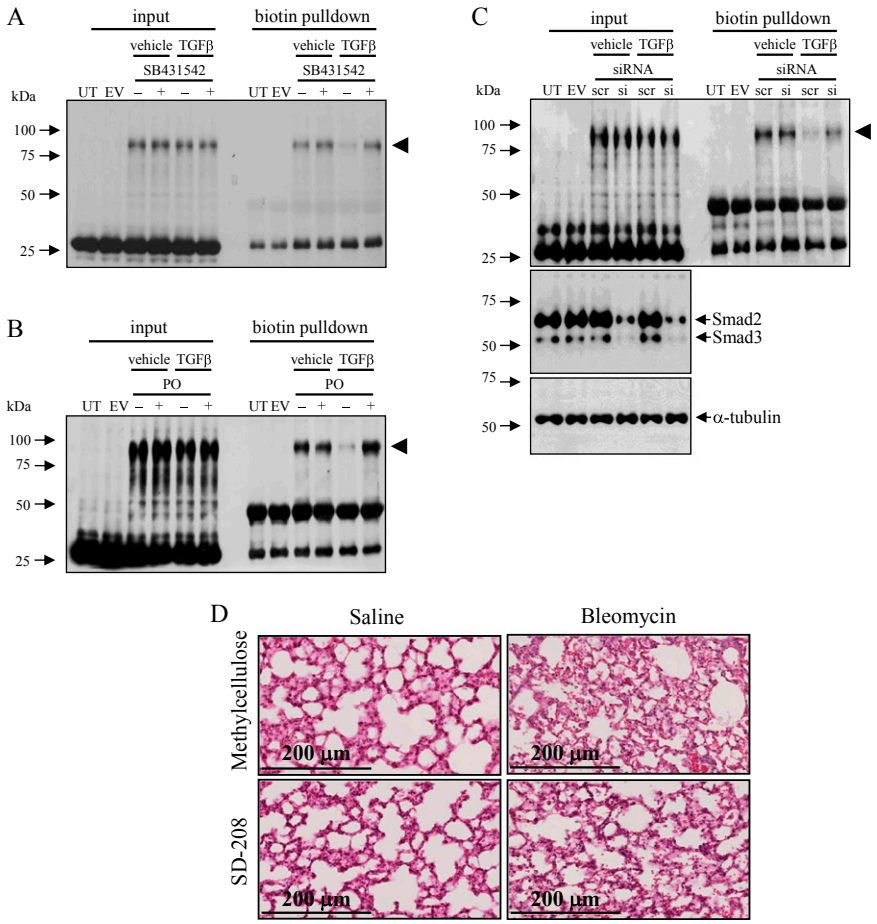

Fig. S5. TGF-β drives ENaC internalization in a Tgfbr1/Smad2/3-dependent pathway that relies on actin mobility. Effects of (*A*) the Tgfbr1 inhibitor SB431542 (10 μM), (*B*) PO (10 μM), an inhibitor of actin mobility, and (*C*) Smad2/3 knockdown by small-interfering (si)RNA [or scrambled (scr) siRNA], on endocytosis of V5-tagged βENaC (arrowhead) in A549 cells stimulated with TGF-β (10 ng/mL). (*D*) Representative H&E-stained lung sections from the four treatment groups of mice: which were treated intratracheally either with saline (as control) or bleomycin to induce lung injury, and concomitantly with methylcellulose (as vehicle) or the Tgfbr1 kinase inhibitor SD-208 dissolved in methylcellulose, which were administered by oral gavage.

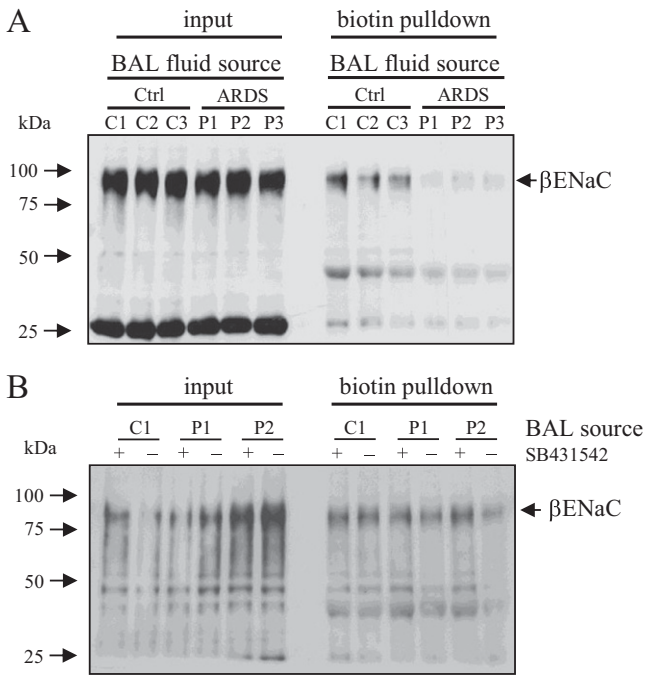

Fig. S6. TGF-β is the active principle in BAL fluids from patients with ARDS that promotes ENaC endocytosis. (*A*) Effects of BAL fluid from three control patients (designated C1, C2, and C3) and three ARDS patients (designated P1, P2, and P3) on βENaC endocytosis in A549 cells, assessed as described in the legend to Fig. S2. (*B*) Ability of SB431542 to block BAL fluid-induced βENaC endocytosis by A549 cells. In control lanes (–), the SB431542 was replaced by vehicle alone [0.1% (vol/vol) dimethyl sulfoxide]. These data are quantified in Fig. 4*D*.

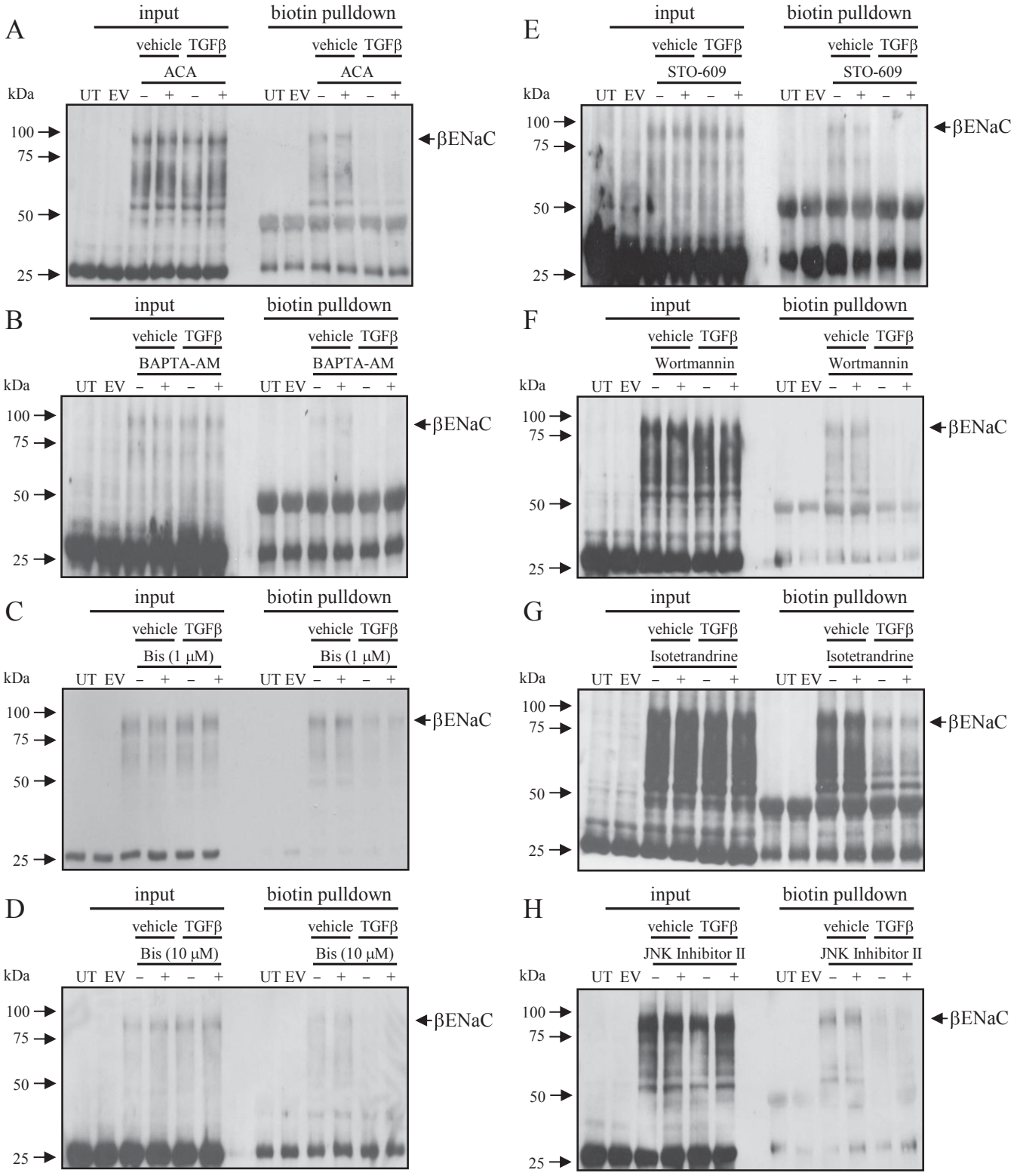

Fig. S7. Screening pathway inhibitors for impact on TGF-β–induced ENaC endocytosis. A549 cells expressing V5-tagged human βENaC were treated with a spectrum of signaling pathway inhibitors before treatment with TGF-β (TGFβ; 10 ng/mL): (*A*) the phospholipase A2 inhibitor, *N*-(*p*-amylcinnamoyl)anthranilic acid (25 μM); (*B*) the membrane-permeable intracellular Ca^{2+}-chelator BAPTA-AM (25 mM); (*C*) the protein kinase C inhibitor, bisindolylmaleimide I (1 μM); (*D*) the protein kinase C inhibitor, bisindolylmaleimide I (10 μM); (*E*) the Ca^{2+}/calmodulin-dependent protein kinase kinase inhibitor, STO-609 (20 μg/mL); (*F*) the phosphoinositide-3 kinase inhibitor, wortmannin (100 nM); (*G*) the phospholipase A inhibitor, isotetrandrine (1 μg/mL); and (*H*) the c-jun N-terminal kinase inhibitor II (50 μM). Total cellular levels are evident in input lanes and cell-surface abundance was assessed by cell-surface biotinylation, pull-down, and immunoblot on the same membrane. Cells were pretreated with brefeldin A (10 μg/mL), and were untransfected (UT), transfected with empty vector (EV), or transfected with a construct expressing V5-tagged human βENaC.

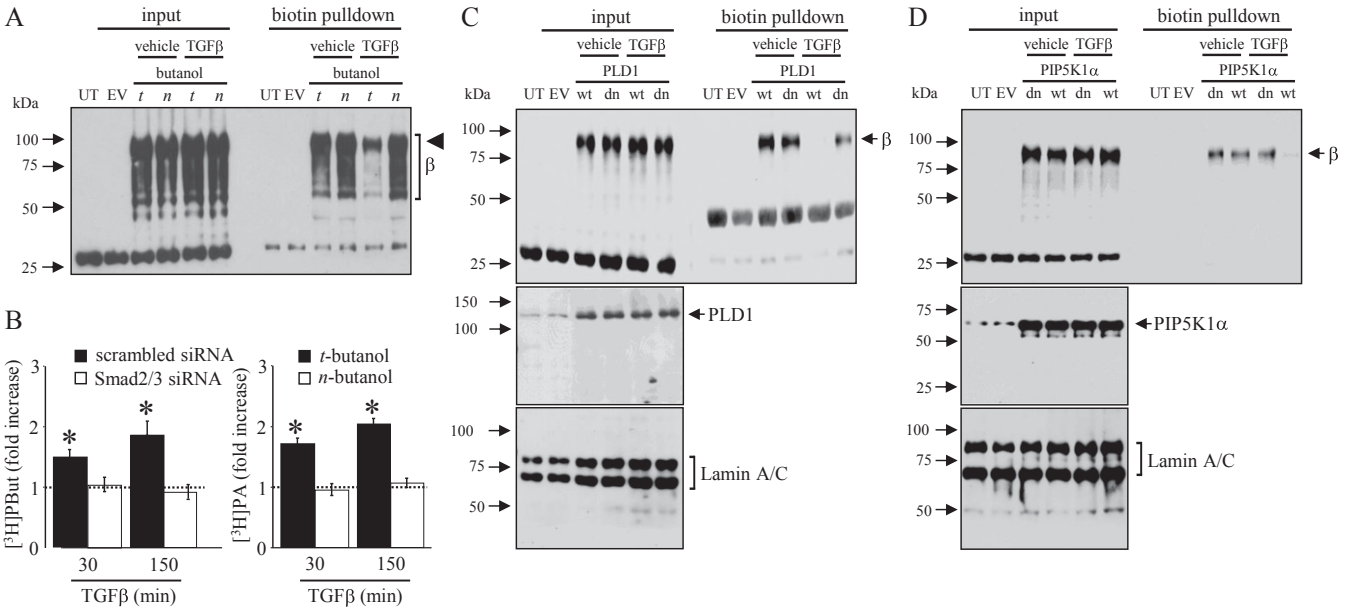

Fig. S8. TGF-β activation of PLD1 and PIP5K1α is required for βENaC endocytosis. The impact of (*A*) l-butanol [*n*; 0.1% (vol/vol); a PLD inhibitor] or *t*-butanol [*t*; 0.1% (vol/vol); control, which is not a substrate for transphosphatidylation] on βENaC (arrowhead) endocytosis by A549 cells in response to TGF-β (10 ng/mL) assessed by biotin pull-down. The bracket indicates the βENaC smear (β). (*B*) Production of PBut and PA in A549 cells treated as described for *A*, and stimulated with TGF-β. Data represent mean ± SD ($n = 5$). *$P < 0.05$. (*C*) The impact of overexpression of wild-type (wt) or a dominant-negative (dn) variant of PLD1 on βENaC endocytosis by A549 cells in response to TGF-β was assessed by biotin pull-down as described in the legend to Fig. S2. (*D*) The impact of overexpression of wild-type (wt) or a dominant-negative (dn) variant of *PIP5K1A* on βENaC endocytosis by A549 cells in response to TGF-β was assessed by biotin pull-down. UT; untransfected; EV, empty vector-transfected.

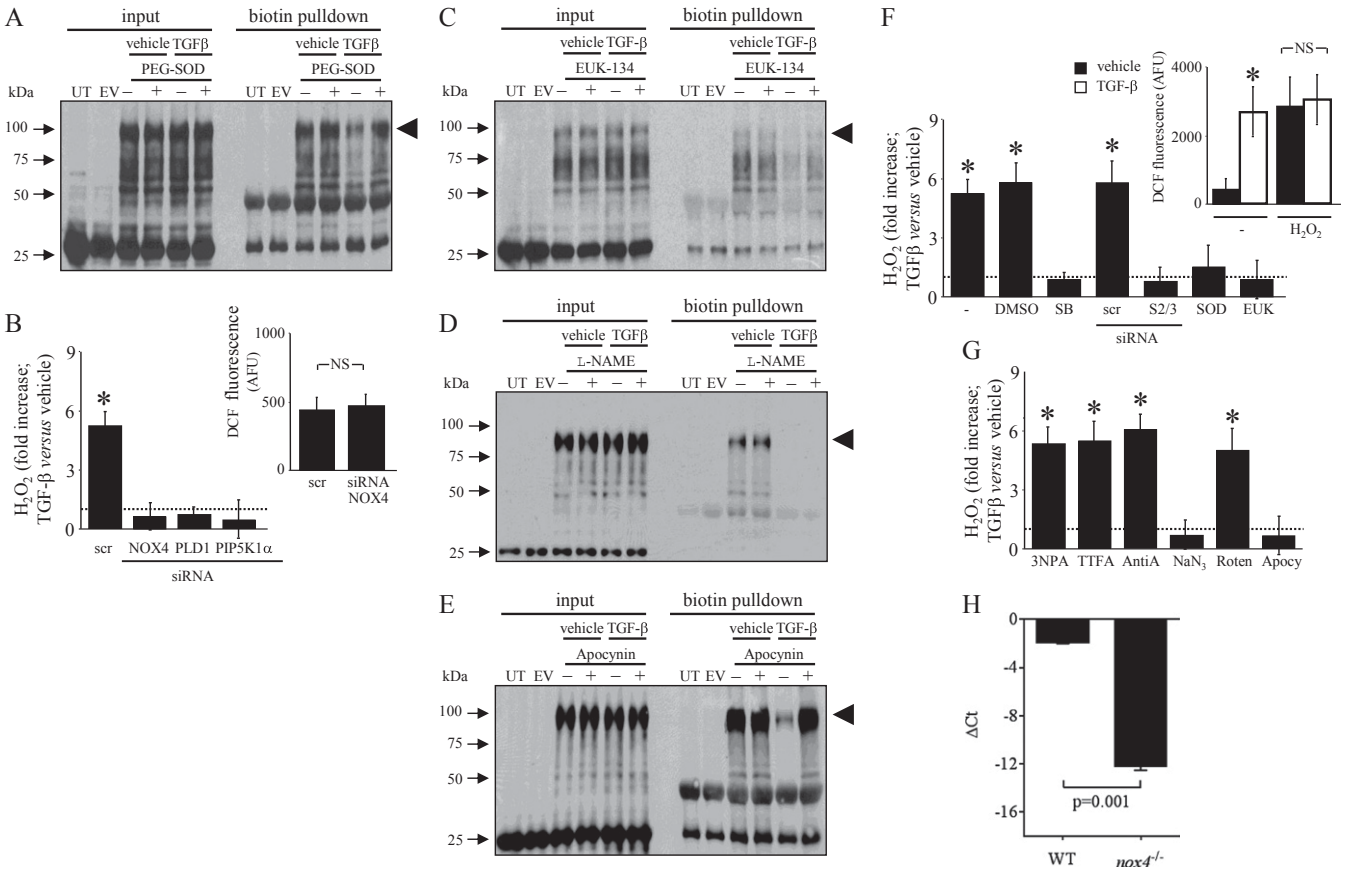

Fig. S9. TGF-β–generated ROS are required for βENaC endocytosis. (*A*) Effects of the ROS scavenger polyethylene glycol (PEG)-complexed superoxide dismutase (SOD) on TGF-β-driven βENaC endocytosis by A549 cells. (*B*) Effects of genetic ablation of *NOX4*, *PLD1*, and *PIP5K1A* by siRNA on TGF-β–induced ROS production by A549 cells, and the effect of *NOX4* knockdown on baseline ROS levels (*Inset*) ($n = 3$, per group). The effects of the ROS scavenger EU.K.-134 (*C*), the nitric oxide synthase inhibitor L-NAME (100 mM) (*D*), and apocynin (300 μM) (*E*) on TGF-β–driven βENaC internalization by A549 cells was also assessed. UT; untransfected; EV, empty vector-transfected. (*F*) TGF-β pathway inhibitors and ROS scavengers were assessed for effects on TGF-β–induced ROS production (measured as H_2O_2) by A549 cells: untreated (–), or treated with DMSO [0.1% (vol/vol)]; SB431542 (SB; 10 μM); scrambled small-interfering (si)RNA (scr), siRNA targeting Smad2 and Smad3 (S2/3); PEG-complexed SOD (SOD; 150 U/mL); or EU.K.-134 (EU.K.; 20 μM). Arbitrary fluorescence units (AFU) obtained with untreated or TGF-β–treated naïve cells, without (–) or with addition of 100 μM H_2O_2 as positive control ($n = 3$, per group; *Inset*). (*G*) Inhibitors of the electron transport chain and NADPH oxidases were assessed for effects on TGF-β–induced ROS production by A549 cells: 3-nitropropionic acid (3NPA; 5 mM), theonyltrifluoroacetone (TTFA; 10 μM), antimycin A (AntiA; 3 μg/mL), rotenone (Roten; 10 μM), NaN_3 (1 mM), and apocynin (300 μM; Apocy) ($n = 5$, per group). Data represent mean ± SD ($n = 3$, per group). *$P < 0.05$. UT; untransfected; EV, empty vector-transfected, Lam, laminin A/C. (*H*) Confirmation of genetic ablation of Nox4 expression in *nox4*$^{-/-}$ mice, assessed by real-time RT-PCR using mRNA pools from whole-lung homogenates from wild-type and *nox4*$^{-/-}$ mice. Data represent mean ± SD ($n = 5$, per group).

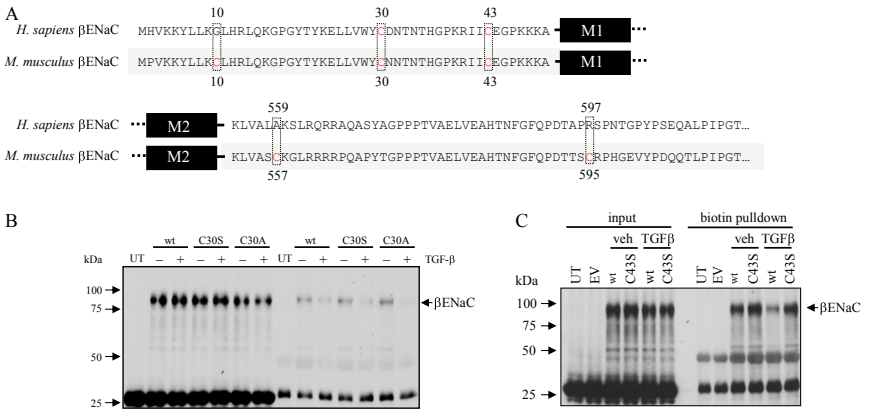

Fig. S10. TGF-β signaling targets Cys[43] of βENaC in mouse and human cells. (*A*) Comparison of the amino acid sequences of the cytosolic domains [regions proximal to the first transmembrane (M1) domain, and distal to the second transmembrane domain (M2)] of human and mouse βENaC. (*B*) The impact of Cys[43] replacement with serine on human βENaC endocytosis by A549 cells in response to TGF-β (10 ng/mL; 30 min) was assessed by biotin pull-down. wt, wild-type. (*C*) The impact of Cys[30] residue replacement to serine or alanine on human βENaC endocytosis by A549 cells in response to TGF-β (10 ng/mL; 30 min) was assessed by biotin pull-down.

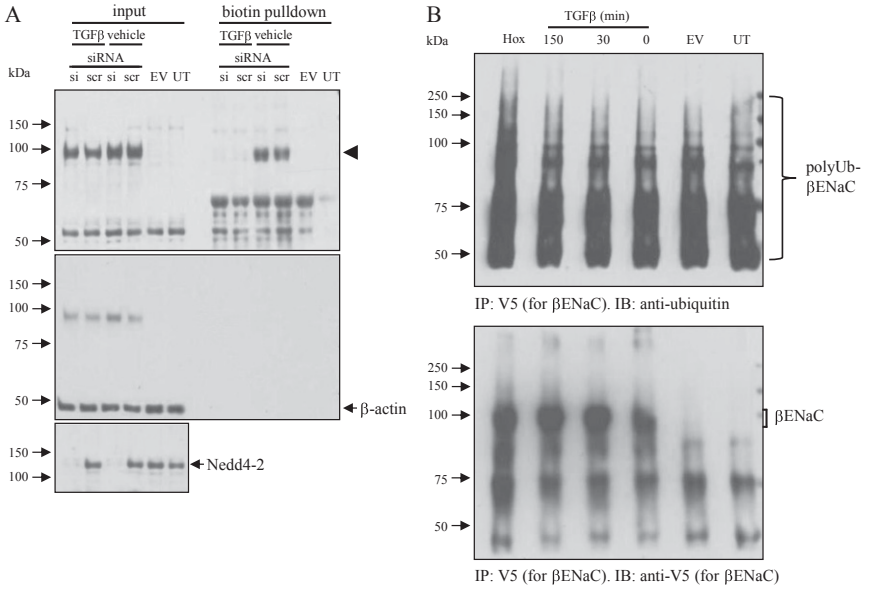

Fig. S11. Nedd4-2-mediated ubiquitination does not play a role in the effects of TGF-β in ENaC trafficking. (*A*) Knockdown of Nedd4-2 by siRNA did not impact the ability of TGF-β to drive internalization of βENaC (*Top*). In this instance, the βENaC blot was reprobed for β-actin to validate that the biotinylation procedure only detected surface-bound material. The β-actin band is only evident in the input, not the pull-down lane, and some residual βENaC signal is still evident in the input as well (*Middle*). The siRNA-mediated knockdown of Nedd4-2 was validated by immunoblot (*Bottom*). (*B*) To support the data presented in *A*, the ubiquitination status of βENaC was also assessed by immunoprecipitation of V5-tagged βENaC, followed by probing for ubiquitin (*Upper*). No increase in poly-ubiquitinated βENaC was evident in the smear indicated; however, hypoxia (1% O_2, 4,5 h), which has been recognized as a stimulus for Nedd4-2–mediated ubiquitination of ENaC (1) did appreciably increase the intensity of the poly-ubiquitinated βENaC smear. The blot was reproved for V5-tagged βENaC (*Lower*). UT, untransfected; EV, empty vector-transfected.

1. Gille T, et al. (2013) Hypoxia-induced inhibition of ENaC in the lung: Role of Nedd4-2 and the ubiquitin-proteasome pathway. *Am J Respir Cell Mol Biol*, in press.

Table S1. Primers used in this study

Gene	Application	Forward primer	Reverse primer
nox4	Expression analysis	5′-GGGATTTGCTACTGCCTCCA-3′	5′-GAGTGACTCCAATGCCTCCA-3′
scnn1a (αENaC)	Expression analysis	5′-GTGTGCATTCACTCCTGC-3′	5′-CTGCACGGCTTCCTGCAC-3′
scnn1b (βENaC)	Expression analysis	5′-GACAAGCTGCAACGCAAG-3′	5′-GGAAGTCCCTGTTGTTGC-3′
scnn1g (γENaC)	Expression analysis	5′-CCACCAGCTTGGCACAGT-3′	5′-ACTGTTGGCTGGGCTCTC-3′
SCNN1A (αENaC)	Expression analysis	5′-ggtggactggaaggactggaagatcg-3′	5′-atgaagttgcccagcgtgtcctcctc-3′
SCNN1B (βENaC)	Expression analysis	5′-ttcatcaggacctacttgagctgg-3′	5′-ggcattggcatggcttagctcaggag-3′
SCNN1G (γENaC)	Expression analysis	5′-ctggagctaaggtgatcatccatcg-3′	5′-gcagcgttgtagatgttcctgattg-3′
hprt	Expression analysis	5′-GATGATCTCTCAACTTTA-3′	5′-AGTCTGGCCTGTATCCAA-3′
HPRT	Expression analysis	5′-AAGGACCCCACGAAGTGTTG-3′	5-GGCTTTGTATTTTGCTTTTCCA-3′
SCNN1A (αENaC)	Cloning	5′-CTCGAGATGGAGGGGAACAAGCTGGAG-3′	5′-CTCGAGGGGCCCCCCCAGAGGACAGGT-3′
SCNN1B (βENaC)	Cloning	5′-CCGCGGatgcacgtgaagaagtacctg-3′	5′- CCGCGGGATGGCATCACCCTCACTGTC-3′
SCNN1G (γENaC)	Cloning	5′-ctcgagatggcacccggagagaagatc-3′	5′-CTCGAGGAGCTCATCCAGCATCTGGGT-3′
pCMV-Tag4B (vector)	Site-directed mutagenesis	5′-GATACCGTCGACACCGGTTAATACAAGGATGAC-3′	5′-GTCATCCTTGTATTAACCGGTGTCGACGGTATC-3′
scnn1b (βENaC C10A)	Site-directed mutagenesis	5′-AAGTACCTCCTGAAGGCCCTGCACCGGCTGCAG-3′	5′-CTGCAGCCGGTGCAGGGCCTTCAGGAGGTACTT-3′
scnn1b (βENaC C10S)	Site-directed mutagenesis	5′-AAGTACCTCCTGAAGAGCCTGCACCGGCTGCAG-3′	5′-CTGCAGCCGGTGCAGGCTCTTCAGGAGGTACTT-3′
scnn1b (βENaC C30A)	Site-directed mutagenesis	5′-CTGCTAGTGTGGTACGCCAATAACACCAACACC-3′	5′-GGTGTTGGTGTTATTGGCGTACCACACTAGCAG-3′
scnn1b (βENaC C30S)	Site-directed mutagenesis	5′-CTGCTAGTGTGGTACAGCAATAACACCAACACC-3′	5′-GGTGTTGGTGTTATTGCTGTACCACACTAGCAG-3′
scnn1b (βENaC C43A)	Site-directed mutagenesis	5′-CCCAAACGCATCATCGCTGAGGGGCCCAAGAAG-3′	5′-CTTCTTGGGCCCCTCAGCGATGATGCGTTTCCC-3′
scnn1b (βENaC C43S)	Site-directed mutagenesis	5′-CCCAAACGCATCATCAGTGAGGGGCCCAAGAAG-3′	5′-CTTCTTGGGCCCCTCACTGATGATGCGTTTCCC-3′
scnn1b (βENaC C557A)	Site-directed mutagenesis	5′-AAGCTGGTGGCCTCCGCCAAAGGCCTGCGCAGG-3′	5′-CCTGCGCAGGCCTTTGGCGGAGGCCACCAGCTT-3′
scnn1b (βENaC C557S)	Site-directed mutagenesis	5′-AAGCTGGTGGCCTCCAGCAAAGGCCTGCGCAGG-3′	5′-CCTGCGCAGGCCTTTGCTGGAGGCCACCAGCTT-3′
scnn1b (βENaC C595A)	Site-directed mutagenesis	5′-CCTGACACAACCAGCGCCAGGCCCCACGGCGAG-3′	5′-CTCGCCGTGGGGCCTGGCGCTGGTTGTGTCAGG-3′
scnn1b (βENaC C595S)	Site-directed mutagenesis	5′-CCTGACACAACCAGCAGCAGGCCCCACGGCGAG-3′	5′-CTCGCCGTGGGGCCTGCTGCTGGTTGTGTCAGG-3′
SCNN1B (βENaC C30S)	Site-directed mutagenesis	5′-CTGCTGGTGTGGTACTCCGACAACACCAACACC-3′	5′-GGTGTTGGTGTTGTCGGAGTACCACACCAGCAG-3′
SCNN1B (βENaC C43S)	Site-directed mutagenesis	5′-CCCAAGCGCATCATCTCTGAGGGGCCCAAGAAG-3′	5′- CTTCTTGGGCCCCTCAGAGATGATGCGCTTGGG-3′

By convention, mouse genes are indicated in lowercase, and human genes in uppercase. Engineered restriction sites are indicated in bold type, and engineered stop-codons are underlined.